Laura Hellwege*, Moritz Schaar, Thorsten M. Buzug, and Maik Stille

Enhancing virtual monoenergetic images for non-congruent dual-energy CT projection data

https://doi.org/10.1515/cdbme-2023-1169

Abstract: This study investigates the application of joint bilateral filtering for noise reduction in fast kVp switching dual-energy computed tomography (DECT). A high resolution image is calculated from non-congruent data of two scans with different energy spectra. This image guides the denoising process of the material decomposition that are used to obtain virtual monoenergetic images (VMIs). The performance of the filter was evaluated in terms of standard deviations on measured data. The proposed filter significantly reduces noise in the VMIs and preserves edges. Furthermore, the simple implementation of the filter can be used for various scanning protocols.

Keywords: image reconstruction, computed tomography, dual energy, joint bilateral filter, fast kVp switching

1 Introduction

Dual-energy computed tomography is an advanced imaging technique that allows for material decomposition by using two different energy spectra to scan an object. The resulting data can be decomposed in basis materials and re-combined to eliminate beam hardening and obtain high-quality, artifact-free images. For the material decomposition several methods are available [1].

With the rise of photocounting detectors spectral reconstruction is now gaining more research interest especially in combination with statistical iterative algorithms [2]. However, increased development effort and production costs limit access to these machines. On the other hand, DECT scanners based on dual source systems, multi-layer detectors or fast kilovolt switching methods are more common and can be fine tuned to generate high quality data.

One advantage of DECT over conventional single energy CT is the possibility of material decomposition of the measured object as well as the generation of virtual monoenergetic images. Therefore, either extensive knowledge of each scanner component is required or a sophisticated calibration strategy has to be implemented to obtain scanner parameters for material decomposition. One major drawback of material decomposition is noise amplification [3]. In the study presented we investigate the application of a joint bilateral filter for noise reduction in material decomposition for DECT data from non-congruent views.

***Corresponding author: Laura Hellwege,** Institute of Medical Engineering, University of Lübeck, Ratzeburger Allee 160, Lübeck, Germany, E-mail: l.hellwege@uni-luebeck.de
Moritz Schaar, Thorsten M. Buzug, Maik Stille, Fraunhofer Research Institution for Individualized and Cell-Based Medical Engineering, Lübeck, Germany

2 Methods

Material decomposition

Alvarez and Macovski have shown in [4] that the linear attenuation coefficients $\mu_j, j \in \{1, ..., N\}$, with $N \in \mathbb{N}$ voxels at energy E can be expressed as

$$\mu_j(E) = \mu^{m_1}(E) \cdot \alpha_j^{m_1} + \mu^{m_2}(E) \cdot \alpha_j^{m_2},$$

where $\mu^{m_1}(E)$ and $\mu^{m_2}(E)$ represent the theoretical linear attenuation coefficients of two basis materials m_1 and m_2. These are combined with the basis material images $\alpha_j^{m_1}$ and $\alpha_j^{m_2}$. Since theoretical values are known, the main challenge in DECT is the computation of the basis material images.

Empirical dual-energy calibration

Empirical dual-energy calibration (EDEC) [5] can be used to implicitly obtain scanner parameters during a calibration procedure of two known objects. Thereby, monochromatic reconstructions $f = [f_1, ..., f_N]^T$ can be computed from the polychromatic CT data y^{s_1} and y^{s_1} with $y^{\cdot} \in \mathbb{R}^{N_p \times N_d}$ using two different X-ray spectra s_1 and s_2, with N_p being the number of projections and N_d the total number of detector pixels. The basis material image $f^{\cdot}$ is obtained by a linear combination of the basis images $\{B_m \in \mathbb{R}^N \,|\, m = 1, ..., M\}$ and their respective coefficients $\mathbf{c}^{\cdot} = \{c_m^{\cdot} \in \mathbb{R} \,|\, m = 1, ..., M\}$ as

$$f_j^{\cdot}(\mathbf{c}^{\cdot}) = \left(\sum_{m=1}^{M} c_m^{\cdot} \cdot R^{-1}\{b_m(y^{s_1}, y^{s_2})\} \right)_j = \left(\sum_m c_m \cdot B_m \right)_j,$$

where R^{-1} indicates the three-dimensional inverse Radon transform and the index $\cdot$ indicates one of the chosen basis materials. The calibration can be performed either in projection or

image domain. Although projection-based methods generally outperform image-based methods in terms of artifact reduction and quality of the reconstructed images, data from congruent views is required. In the case of non-congruent data, only image-based methods can be applied. For the problem at hand an additive basis

$$b_m(y^{s_1}, y^{s_2}) = (y^{s_1})^{m_1} + (y^{s_1})^{m_2}$$

is used with $m = m_1(M^\star + 1) + m_2$ but $m_1 = 0$ if $m_2 \neq 0$ and $m_2 = 0$ if $m_1 \neq 0$ with $m_1, m_2 = 0, ..., M^\star$ [5]. In this work, $M^\star = 2$ is chosen for all evaluations. This results in $M = (M^\star + 1)^2 = 9$ basis images and coefficients per basis material.

For EDEC, two template images $t^{\cdot}$ - one for each basis material - and a weight image w are required and used in the optimization of the coefficients $\mathbf{c}^{\cdot}$. We obtained these images as shown in Figure 1 by simple thresholding and morphological operations. As described in [5] for the continuous case, the discretized calibration shall then minimize the data term

$$E(\mathbf{c}^{\cdot}) = \sum_{j=1}^{N} w_j \cdot (f_j^{\cdot}(\mathbf{c}^{\cdot}) - t_j^{\cdot})^2,$$

where $t^{\cdot}$ serves as a template image and w adds capabilities for weighting image areas differently. The minimization is then achieved by constructing and solving a linear system of equations. More information on the general procedure can be found in [5].

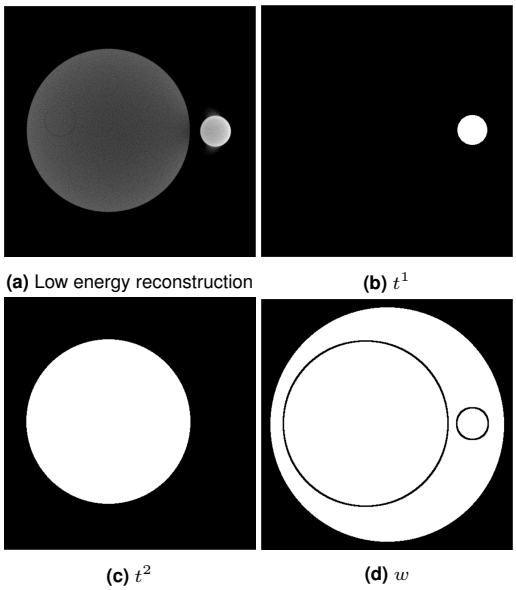

Fig. 1: Template images (b) t^1 and (c) t^2 and (d) weight image w created from the polychromatic low energy image reconstruction (a) and the field-of-view that is given by the system geometry.

Joint bilateral filter

In the case of non-congruent data, both projection datasets can be used to complement each other by reconstructing all acquired projections into one image regardless of the energy used for acquisition. At best, this doubles the number of projections when both sets of viewing angles are offset by one half of the angular increment. This results in an image of average intensity, due to the energy mismatch of both scans, which is physically incorrect, but has the capability to enhance edges and reduce noise. We are using this average image as guidance in a joint bilateral filter (JBF) as proposed in [6] to reduce the noise of the material decomposed images.

The calculation of the voxel f_j^{filtered} of the filtered image is defined as

$$f_j^{\text{filtered}} = \frac{\sum_{k=1}^{N} w^g(j,k) \cdot f_k}{\sum_{k=1}^{N} w^g(j,k)}, \text{with} \quad (1)$$

$$w^g(j,k) = \exp\left(-\frac{(g_j - g_k)^2}{2\sigma_{\text{I}}^2} - \frac{\|j-k\|^2}{\sigma_{\text{S}}^2}\right). \quad (2)$$

Equation 2 incorporates the information of the guiding image g into the filter equation 1 by an exponential term of two arguments: The first exponent is influenced by the intensity differences of the guiding image, the second term by the spatial distance of the two voxels j and k. The two filter parameters $\sigma_I \in \mathbb{R}_{>0}$ and $\sigma_S \in \mathbb{R}_{>0}$ are used to weight the respective component. For a comparison of the proposed method, we employ the conventional bilateral filter. In this case, the guiding image is then the image to be filtered itself.

Measurements

We acquired two dual-energy scans; one for calibration and one for evaluation. Two cylindrical phantoms were used as calibration objects: The first custom-made cylinder consists of 150 mm diameter polymethyl-methacrylate (PMMA), the second cylinder has a diameter of 28 mm and is made of calcium (300 mg/mL). Both cylinders have a height of 200 mm. The arrangement of the calibration phantoms is shown in Figure 1 (a). All tissue mimicking cylinders that are used are part of the Gammex Multi-Energy CT Phantom (Sun Nuclear Corporation). For evaluation, a set of five cylinders was placed inside a water-filled container. Here, we used calcium (100 mg/mL and 50 mg/mL), adipose, blood (70 mg/mL), and solid water. The arrangement of the cylinders can be seen in Figure 2.

Measurements were performed on a YXLON FF35 CT equipped with a Varex XRD 4343CT flat-panel detector and 225 kV directional tube. Per spectrum, we acquired 360 projections with 1.0° angular increment. The measured data had an angular difference of 0.5° between the low-energy and the high-energy spectrum. We used 3 × 3 binning that results in a projection size of 954 × 954 pixels with spacing of 0.45 mm. Source-to-detector distance was 1000 mm and

source-to-isocenter distance was 500 mm. Two spectra were employed for data acquisition. The low energy scan was performed with 90 kVp and an additional filter of 3.5 mm aluminium in front of the source. For the high energy spectrum 150 kVp with 2.0 mm copper was chosen.

Images were reconstructed using Feldkamp-David-Kress reconstruction (FDK) with a cut-off frequency of 0.7 for the Hann-Filter in our in-house reconstruction software that is based on the Reconstruction Toolkit (RTK) [7]. Images were reconstructed on a grid with 512 × 512 × 512 voxels and 0.4 mm isotropic voxel size.

Evaluation

To analyze the noise reduction capabilities of the proposed filter, we calculated standard deviations in three regions-of-interest (ROIs) over a set of different VMI reference energies. For calcium (50 mg/mL) and adipose we defined cylindrical ROIs as shown in Figure 4 that are slightly smaller than the actual cylinders to reduce the influence of partial volume effects. For water we calculated a ROI that was smaller than the water-filled container reduced by the size of the non-water inserts. Note that this ROI is considerably larger than the others.

3 Results

Figure 2 shows the resulting VMIs of conventional EDEC in (a) as well as the high resolution image used as guidance for the joint bilateral filter (b). The results of the bilateral filter with $\sigma_I = 0.01$ and $\sigma_S = 0.75$ mm are shown in (c). Subfigure (d) shows the results of the joint bilateral filter with $\sigma_I = 0.005$ and $\sigma_s = 0.75$ mm. It can be seen that the guidance image has significantly higher quality in terms of noise compared to the single scan results. On the other hand, the contrast is reduced due to the averaging of the data. Whereas the conventional bilateral filter only slightly reduces noise, the impact of the joint bilateral filter is clearly visible. The difference images shown in (e) and (f) emphasize the edge preserving features of both filters and highlight the superior performance of the joint filter. The line profile shown in Figure 3 clearly demonstrates the noise reduction capability. Remaining beam hardening artifacts can be seen towards the edges of the profile. This issue can be attributed to the image-based decomposition method presented and can be seen as systematic errors.

Figure 3 also shows that the location of the mean values is not altered by the application of the filters. To quantify the noise reduction we calculated standard deviations over three VMI reference energies (50, 70 and 100 kV) for all three cases in different ROIs filled with homogeneous materials. The results are shown in Figure 4. It can be seen that the proposed

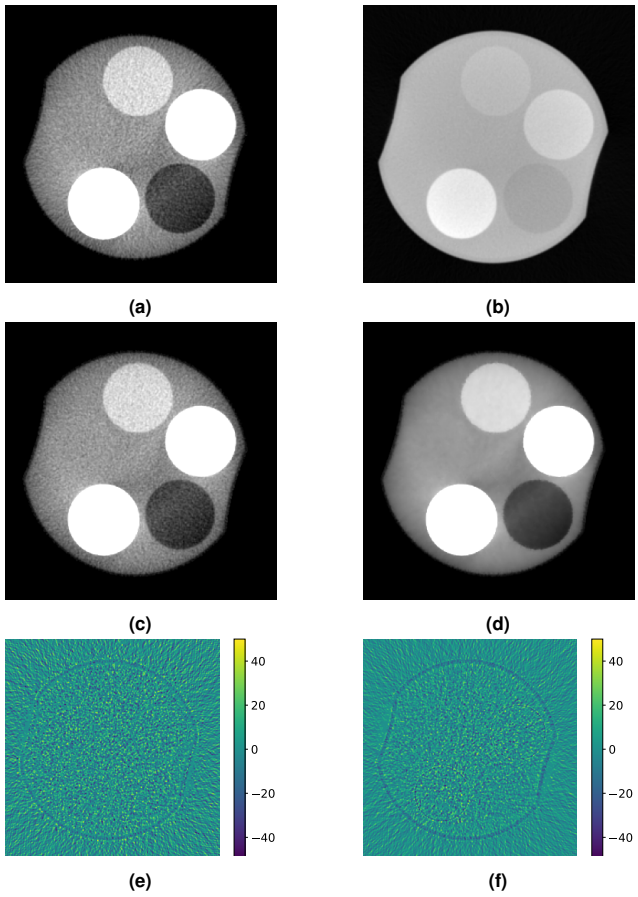

Fig. 2: Reconstructed images at reference energy of 50 kV (L: 0 HU, W: 300 HU): **(a)** unfiltered image, **(b)** high resolution guidance image, **(c)** bilateral filter, **(d)** joint bilateral filter with (b) as guidance image. **(e)** Difference image between unfiltered and filtered image with bilateral filter. **(f)** Difference image between unfiltered and filtered image with JBF.

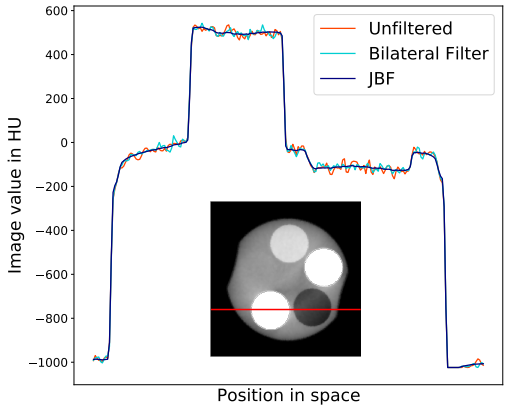

Fig. 3: Line profile through unfiltered and both filtered images as shown in Figure 2 along the highlighted red line.

joint bilateral filter outperforms all other methods in terms of standard deviations. The conventional bilateral filter slightly improves the noise levels for 50 kV but fails to reduce the

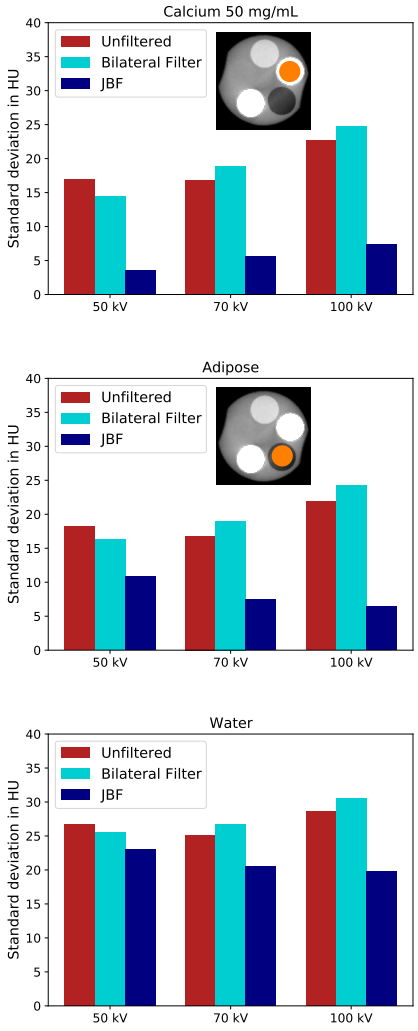

Fig. 4: Standard deviations of different materials in the VMIs of 50, 70 and 100 kV. ROIs are highlighted a orange circles. For water, almost the entire water background in the large cylinder was used.

noise sufficiently for 70 and 100 kV. This might be due to the fact that the material images are recombined after filtering to form the VMI. If the guiding image for both filter applications is not the same, this might introduce new noise in the afterwards combined image. For water, the standard deviation is significantly larger than for adipose and calcium. This can be attributed to the large ROI that also contains some residual artifacts of the image-based material decomposition.

4 Conclusion

The study demonstrates the effectiveness of a proposed filter in reducing noise and preserving edges in the computed VMIs. The research highlights the importance of choosing the appropriate filter as the naive application of the bilateral filter can worsen the noise level in homogeneous areas. The proposed joint bilateral filter, on the other hand, reliably reduces noise in the images and can be easily integrated into existing DECT imaging methods like EDEC.

The proposed filter has important clinical applications in a range of diagnostic or interventional procedures that involve non-congruent projection data. However, the filter parameters were manually selected in this work, and future advancements should focus on automatic estimation or tuning of these values from the available data.

Further research is also needed to quantify the proposed approach on other phantoms and evaluate it in a more qualitative manner for medically relevant anatomies. The results of such studies will enhance the understanding of the proposed filter's potential in improving the accuracy and reliability of DECT imaging methods, ultimately benefiting patient care.

Author Statement

The project was funded by the German Federal Ministry of for Education and Research under the funding code 13GW0371C.

References

[1] Patino M, Prochowski Iamurri A, Agrawal M, Simeone F, Gupta R, Hahn P, Sahani D. Material Separation Using Dual-Energy CT: Current and Emerging Applications. Radiographics : a review publication of the Radiological Society of North America, 2016;36:1087-1105.

[2] Weidinger T, Buzug T M, Flohr T, Kappler S, Stiersdorfer K. Polychromatic Iterative Statistical Material Image Reconstruction for Photon-Counting Computed Tomography. Int J Biomed Imaging 2016;2016:5871604.

[3] Kalender W A, Klotz E, Kostaridou L. An algorithm for noise suppression in dual energy CT material density images. IEEE Trans Med Imaging 1988;7.3:218-224.

[4] Alvarez R E, Macovski A. Energy-selective reconstructions in x-ray computerised tomography. Phys Med Biol 1976;21.5:733-744.

[5] Stenner P, Berkus T, Kachelriess M. Empirical dual energy calibration (EDEC) for cone-beam computed tomography. Med Phys 2007;34.9:3630-3641.

[6] Petschnigg G, Szeliski R, Agrawala M, Cohen M, Hugues H, Toyama K. Digital photography with flash and no-flash image pairs. ACM Trans Graph 2004;23.3:664-672.

[7] Rit S, Vila Oliva M, Brousmiche S, Labarbe R, Sarrut D, Sharp G C. The Reconstruction Toolkit (RTK), an open-source cone-beam CT reconstruction toolkit based on the Insight Toolkit (ITK). J Phys Conf Ser 2014;489.1:012079.